

# Extraction of bridge aeroelastic parameters by one reference-based stochastic subspace technique

F.Y. Xu<sup>\*1</sup>, A.R. Chen<sup>2</sup>, D.L. Wang<sup>2</sup> and R.J. Ma<sup>2</sup>

<sup>1</sup>School of Civil Engineering, Dalian University of Technology, Dalian 116024, China

<sup>2</sup>Department of Bridge Engineering, Tongji University, Shanghai 200092, China

(Received July 8, 2010, Accepted March 9, 2011)

**Abstract.** Without output covariance estimation, one reference-based Stochastic Subspace Technique (SST) for extracting modal parameters and flutter derivatives of bridge deck is developed and programmed. Compared with the covariance-driven SST and the oscillation signals incurred by oncoming or signature turbulence that adopted by previous investigators, the newly-presented identification scheme is less time-consuming in computation and a more desired accuracy should be contributed to high-quality free oscillated signals excited by specific initial displacement. The reliability and identification precision of this technique are confirmed by a numerical example. For the 3-DOF sectional models of Sutong Bridge deck (streamlined) and Suramadu Bridge deck (bluff) in wind tunnel tests, with different wind velocities, the lateral bending, vertical bending, torsional frequencies and damping ratios as well as 18 flutter derivatives are extracted by using SST. The flutter derivatives of two kinds of typical decks are compared with the pseudo-steady theoretical values, and the performance of  $H_1^*$ ,  $H_3^*$ ,  $A_1^*$ ,  $A_3^*$  is very stable and well-matched with each other, respectively. The lateral direct flutter derivatives  $P_5^*$ ,  $P_6^*$  are comparatively more accurate than other relevant lateral components. Experimental procedure seems to be more critical than identification technique for refining the estimation precision.

**Keywords:** bridge; parameter identification; flutter derivative; stochastic subspace technique; wind tunnel test.

## 1. Introduction

Flutter derivatives are critical parameters describing aerodynamic characteristics of bridge deck and predicting the flutter and buffeting performances of long-span flexible bridges. Considerable efforts and valuable researches concerning 2-DOF and 3-DOF experimental techniques and identification algorithms have been made on the determination of aeroelastic derivatives using spring-suspended bridge deck section models in wind tunnels in the last decade. Gu *et al.* (2000), Li *et al.* (2004) and Gianni *et al.* (2009) used Unifying Least Squares (ULS), ensemble ULS, and improved ULS techniques to identify eight flutter derivatives of different bridge decks, and some progresses have been made. Chen *et al.* (2004) highlighted the techniques and implied approximations employed in the literature to identify flutter derivatives from section model studies. Then, the control parameters with a critical influence on the development of inter-modal coupling and the

---

\* Corresponding Author, Assistant professor, E-mail: fuyouxu@hotmail.com

generation of aerodynamic damping were identified based on closed-form solutions of bimodal coupled analysis of bridge aeroelastic system (Chen *et al.* 2008). Chen *et al.* (2006) proposed a Stochastic Search Algorithm (SSA) and improved the identification precision based on the signals preprocessed by Empirical Mode Decomposition (EMD). Chen *et al.* (2010) developed the Sub-section Extended-Order Iterative Least Square (SEO-ILS) algorithm in the state space for direct identification of system matrices from free vibration data of eccentric section models. The eccentricity is found to have more influence on the cross flutter derivatives than on the direct flutter derivatives.

For the reason of the wide and matured study of eight flutter derivatives relevant to vertical and torsional motions, many researchers paid more attention to the identification of eighteen flutter derivatives, emphasizing on those pertinent with the lateral motion. Singh *et al.* (1996) extended the MITD method to extract all 18 flutter derivatives. However, the values of  $H_6^*$ ,  $A_5^*$ ,  $P_3^*$ ,  $P_5^*$ ,  $P_6^*$  are scattered and the precisions are not satisfactory. Chen *et al.* (2002) utilized the general least squares theory and compared the flutter derivatives with those obtained by Computational Fluid Dynamics. Sarkar *et al.* (2004a, 2004b) developed a novel elastic suspension system for the study of the wind tunnel section model, in which 18 flutter derivatives of an airfoil and a bridge deck are extracted by the newly proposed Iterative Least Square approach. The conception and procedure of this innovative method are simple, and convenient for programming. However, if the ideal signals can not be acquired for the noise contamination, the reliability and effectiveness will be seriously impaired. Mishra *et al.* (2006) applied the covariance-driven stochastic subspace technique to identify 18 flutter derivatives of a bridge deck section model in smooth flows. The results have been approximated by the rational functions, and apparent difference between the two sets of corresponding data can be observed. As is known that  $H_1^*$ ,  $H_3^*$ ,  $A_1^*$ ,  $A_3^*$  are quite stable for almost all kinds of wind tunnel tests. Their precision and stability are not ensured from the given graphs. The major reason is not the identification technique, but probably due to the experimental scheme. The quality of oscillation signals excited by signature turbulence in smooth flow is not efficiently ensured. In spite of the objective reality of the comparatively inferior identification results for the lateral flutter derivatives, more attempts should be made to push the ongoing progress for precisely predicting various wind-induced responses of long-span bridges.

The Eigensystem Realization Algorithm (ERA) belongs to one advanced time domain method for system identification. Ma *et al.* (2007) has developed modal parameters and flutter derivatives of taut strip models by using ERA. Qin *et al.* (2007) identified the eight flutter derivatives of one twin-deck and investigated the effects of gap-width. Nevertheless, ERA may not be applicable to the signals with various noises, unless the original signals are preprocessed by using the appropriate digital filtering and Random Decrement technique (Quan *et al.* 2005). The stochastic subspace techniques (SST) seem to be an ideal method for determining bridge deck flutter derivatives based on the free vibration signals excited by ambient oncoming or signature turbulences that acquired in smooth flows (Mishra *et al.* 2006), turbulent wind flows (Qin and Gu 2004, Gu and Qin 2004) or wind-rain-hybrid flows (Gu and Xu 2008). Some active attempts are made for extracting six or eighteen flutter derivatives, and many instructive findings and conclusions are provided by these researchers. The noise subspaces can be effectively separated and removed by SST. The noise-immunity performance of SST is better than that of ERA.

However, the previous SST and experimental scheme adopted by different investigators are characterized by two aspects. The first key aspect is the oscillation amplitudes incurred by oncoming or signature turbulences may be relatively lower than those obtained in the initial

displacement impulse excitation, especially for the signature turbulence case in smooth flows. Therefore, the identification precision may not be effectively ensured, just as presented by Mishra *et al.* (2006). Secondly, they are all based on the covariance-driven technique for estimating the modal parameters, and the time-domain data have to be transformed into the correlation function so as to calculate the covariance matrices, thus the computation is time-consuming.

To circumvent the possible and potential problems for the improvement of identification precision, one reference-based SST (Peeters and Roeck 1999) for identifying system modal parameters and aerodynamic derivatives is developed and programmed in this study. Generally speaking, reference-based SST may not exert its superiorities in most wind tunnel tests with a few measurements. Only in the cases (e.g., field measurement of real long-span flexible bridge and high-rise slender building) that a large amount of signals can not be collected synchronously (e.g., due to lack of adequate sensors), and step-by-step tests have to be conducted, the reference-based SST can conveniently and successfully tackle the formidable issues that can not be handled by other SST. Then, the reliability and identification accuracy is verified by a numerical example before applying to the actual engineering issues. Subsequently, the frequency and damping ratios stabilization diagrams are illustrated for deepening the understanding of SST properties. On this basis, according to the free vibration signals generated by the artificial initial displacement impulse, modal parameters such as the frequencies, damping ratios and 18 flutter derivatives of Sutong Bridge (streamlined deck) and Suramadu Bridge (bluff deck) 3-DOF sectional models are determined by SST. Finally, the results are compared with the pseudo-steady theoretical values, particularly with the lateral flutter derivatives, and a comprehensive analysis is conducted and some meaningful conclusions are drawn.

## 2. Theoretical expression of reference-based SST

### 2.1. Construction of state-space matrix (Peeters 1999)

Assume there are  $l$  measurement points or recorded time histories for a bridge deck section model or full bridge aeroelastic model (lateral, vertical or torsional responses at different locations) in wind tunnel tests (or in shaking table tests and on-site tests), the former  $r$  records serve as references, then at the  $k^{\text{th}}$  time, the output vector of accelerations or displacements can be expressed as

$$y_k = \begin{pmatrix} y_k^{ref} \\ y_k^{-ref} \end{pmatrix} \quad (1)$$

where column vectors  $y_k^{ref} \in R^{r \times 1}$ ,  $y_k^{-ref} \in R^{(l-r) \times 1}$  are the references output and non-references output, respectively. The output matrix appears to be  $y \in R^{l \times m}$ , with the length of  $m$ .

The output measurements are gathered in a block Hankel matrix with  $2i$  block rows and  $j$  columns. The first  $i$  blocks have  $r$  rows, the last  $i$  blocks have  $l$  rows. For statistical reasons, it is assumed that  $j \rightarrow \infty$ . The Hankel matrix can be divided into a “past” reference and a “future” part (a Hankel matrix is a matrix where each antidiagonal consists of the repetition of the same element). The block *Hankel* matrix composed of accelerations or displacements of system output may be rearranged as

$$H \equiv \begin{pmatrix} Y_{0|i-1}^{ref} \\ Y_{i|2i-1} \end{pmatrix} \equiv \begin{pmatrix} Y_p^{ref} \\ Y_f \end{pmatrix} \begin{matrix} \updownarrow \\ \updownarrow \end{matrix} \begin{matrix} ri \text{ "past"} \\ li \text{ "future"} \end{matrix} \in R^{(r+l) \times j} \quad (2)$$

where  $Y_{i|2i-1} = Y_f = \frac{1}{\sqrt{j}} \begin{bmatrix} y_i & y_{i+1} & \dots & y_{i+j-1} \\ y_{i+1} & y_{i+2} & \dots & y_{i+j} \\ \vdots & \vdots & & \vdots \\ y_{2i-1} & y_{2i} & \dots & y_{2i+j-2} \end{bmatrix}$ ,  $Y_{0|i-1}^{ref} = Y_p^{ref} = \frac{1}{\sqrt{j}} \begin{bmatrix} Y_0^{ref} & Y_1^{ref} & \dots & Y_{j-1}^{ref} \\ Y_1^{ref} & Y_2^{ref} & \dots & Y_j^{ref} \\ \vdots & \vdots & & \vdots \\ Y_{i-1}^{ref} & Y_i^{ref} & \dots & Y_{i+j-2}^{ref} \end{bmatrix}$

where  $i$  is the length of ‘Past’ data, i.e., time delay.  $j$  is the length of ‘Future’ data.  $j/i$  should be large enough, e.g.,  $j/i \geq 10$ .

Remark that the output data is scaled by a factor  $1/\sqrt{j}$ . The subscripts of  $Y_{i|2i-1} \in R^{li \times j}$  are the subscript of the first and last element in the first column of the block Hankel matrix. The subscript  $p$  and  $f$  stand for past and future. The matrices  $Y_p^{ref}$  and  $Y_f$  are defined by splitting  $H$  into two parts of  $i$  block rows. Another division is obtained by adding one block row to the past references and omitting the first block row of the future outputs. Because the references are only a subset of the output ( $r \leq l$ ),  $l-r$  rows are left over in this new division. These rows are denoted by  $y_{i|i}^{-ref} \in R^{(l-r) \times j}$ . Then  $H$  can be rewritten as

$$H \equiv \begin{pmatrix} Y_0^{ref} \\ y_{i|i}^{-ref} \\ Y_{i|2i-1} \end{pmatrix} \equiv \begin{pmatrix} Y_p^{ref+} \\ y_{i|i}^{-ref} \\ Y_f \end{pmatrix} \begin{matrix} \updownarrow \\ \updownarrow \\ \updownarrow \end{matrix} \begin{matrix} r(i+1) \\ l-r \\ l(i-1) \end{matrix} \quad (3)$$

Some other matrices need to be defined. Defining the extended observable matrix as

$$O_i \equiv (C \ CA \ CA^2 \ \dots \ CA^{i-1})^T \in R^{li \times 2n} \quad (4)$$

Assume  $A$  and  $C$  to be observable matrices, i.e., all vibration modes of system can be observed according to the output acceleration or displacement signals.

Conducting  $QR$  decomposition to block Hankel matrix  $H$

$$H \equiv \begin{pmatrix} Y_p^{ref} \\ Y_f \end{pmatrix} = RQ^T \quad (5)$$

where  $Q \in R^{i \times j}$  is standard orthogonal matrix,  $Q^T Q = Q Q^T = I_j$  and  $R \in R^{(r+l) \times j}$  is lower triangular matrix.

Since  $(r+l)i < j$ , the zero rows or zero columns in matrix  $R$  can be omitted. The corresponding lines and columns in matrix  $Q$  can also be omitted.

$$H = \begin{matrix} ri \ \updownarrow \\ r \ \updownarrow \\ l-r \ \updownarrow \\ l(r-1) \ \updownarrow \end{matrix} \begin{pmatrix} R_{11} & & & \\ R_{21} & R_{22} & & \\ R_{31} & R_{32} & R_{33} & \\ R_{41} & R_{42} & R_{43} & R_{44} \end{pmatrix} \begin{pmatrix} Q_1^T \\ Q_2^T \\ Q_3^T \\ Q_4^T \end{pmatrix} \begin{matrix} \updownarrow \\ \updownarrow \\ \updownarrow \\ \updownarrow \end{matrix} \begin{matrix} ri \\ r \\ l-r \\ l(i-1) \end{matrix} \quad (6)$$

Further in the algorithm, the  $Q$ -factors will cancel out because of their orthonormality. So they are

unnecessary and the important significance of data reduction can be achieved. Assume all information to predict the ‘future’ data are included in the ‘past’ data, the projection of ‘future’ output line space to ‘past’ output line space can be defined as follows.

$$P_i^{ref} \equiv Y_f / Y_p^{ref} \equiv Y_f Y_p^{ref T} (Y_p^{ref} Y_p^{ref T})^+ Y_p^{ref} \quad (7)$$

$$P_{i-1}^{ref} \equiv Y_f^- / Y_f^{ref+} \equiv Y_f^- Y_f^{ref+ T} (Y_f^{ref+} Y_f^{ref+ T})^+ Y_f^{ref+} \quad (8)$$

Projection matrices can be written as

$$P_i^{ref} = \begin{pmatrix} R_{21} \\ R_{31} \\ R_{41} \end{pmatrix} Q_1^T \in R^{li \times j} \quad (9)$$

$$P_{i-1}^{ref} = (R_{41} \ R_{42}) \begin{pmatrix} Q_1^T \\ Q_2^T \end{pmatrix} \in R^{l(i-1) \times j} \quad (10)$$

Perform SVD to projection matrix  $P_i^{ref}$

$$P_i^{ref} = USV^T = (U_1 \ U_2) \begin{pmatrix} S_1 & 0 \\ 0 & 0 \end{pmatrix} \begin{pmatrix} V_1^T \\ V_2^T \end{pmatrix} = U_1 S_1 V_1^T \quad (11)$$

Projection matrix  $P_i^{ref}$  may be transformed into the product of the observable matrix  $O_i$  and Kalman filtering state series  $\hat{X}_i$ . Similarly, projection matrix  $P_{i-1}^{ref}$  may be transformed into the product of the observable matrix  $O_{i-1}$  and Kalman filtering state series  $\hat{X}_{i+1}$ .

$$P_i^{ref} = (C \ CA \ CA^2 \ \dots \ CA^{i-1})^T \cdot (\hat{x}_i \ \hat{x}_{i+1} \ \hat{x}_{i+2} \ \dots \ \hat{x}_{i+j-1}) = O_i \hat{X}_i \quad (12)$$

$$P_{i-1}^{ref} = (C \ CA \ CA^2 \ \dots \ CA^{i-2})^T \cdot (\hat{x}_{i+1} \ \hat{x}_{i+2} \ \hat{x}_{i+3} \ \dots \ \hat{x}_{i+j}) = O_{i-1} \hat{X}_{i+1} \quad (13)$$

where,  $O_i = U_1 S_1^{1/2}$ ,  $O_{i-1} = O_i(1 : l(i-1), :)$ ,  $X_i = O_i^+ P_i^{ref}$ ,  $\hat{X}_{i+1} = O_{i-1}^+ P_{i-1}^{ref}$

Define the  $i^{\text{th}}$  output series  $Y_{i|i}$  of block matrix as

$$Y_{i|i} = \begin{pmatrix} R_{21} & R_{22} \\ R_{31} & R_{32} & R_{33} \end{pmatrix} \begin{pmatrix} Q_1^T \\ Q_2^T \\ Q_3^T \end{pmatrix} \in R^{l \times j} \quad (14)$$

The least-square solutions of state matrix ( $A$ ) and output matrix ( $C$ ) may be expressed as

$$\begin{pmatrix} A \\ C \end{pmatrix} = \begin{pmatrix} \hat{X}_{i+1} \\ Y_{i|i} \end{pmatrix} \hat{X}_i \quad (15)$$

## 2.2 Modal parameter

State-space matrix  $A$  can be written as

$$A = \Psi \Lambda \Psi^{-1} \quad (16)$$

where  $\Lambda = \text{diag}(\lambda_i^2) \in \mathbb{C}^{2n \times 2n}$  is one diagonal matrix constructed by the complex eigenvalues of the discrete system.  $\Psi \in \mathbb{C}^{2n \times 2n}$  is complex eigenvectors matrix of the system, and each column represents an eigenvector  $\phi_i (i = 1, 2, \dots, 2n)$ .

For the continuous system state matrix  $A_c$ , Eq.(16) may be rewritten as

$$A_c = \Psi_c \Lambda_c \Psi_c^{-1} = \Psi \Lambda_c \Psi^{-1} \quad (17)$$

$$\lambda_c^i = \ln(\lambda_i) / \Delta t \quad (18)$$

where  $\Lambda_c = \text{diag}(\lambda_i^{c2}) \in \mathbb{C}^{2n \times 2n}$  is a matrix composed of complex eigenvalues of the continuous system,  $\Delta t$  is the sampling time interval.

According to the conjugation characteristics of system complex eigenvalues, the circular frequency of  $\omega$  and damping ratio  $\xi$  can be calculated with the following formulas

$$\lambda_c, \lambda_c^* = -\xi\omega \pm j\omega\sqrt{1-\xi^2} \quad (19)$$

$$\omega = |\lambda_c| \quad \xi = -R(\lambda_c) / \omega \quad (20)$$

where,  $|\lambda_c|$  and  $R(\lambda_c)$  are the amplitude and real part of  $\lambda_c$ . According to the accustomed description, the eigenvalues of the continuous system can be directly written as  $\lambda$ .

Modal shape may be written as

$$\Phi = C\Psi \quad (21)$$

The continuous system state equation may be expressed as

$$(\lambda_i^2 M + \lambda_i C + K)\phi_i = 0 \quad (22)$$

Multiplying  $M^{-1}$  at both sides of equation, then

$$(\lambda_i M^{-1} C + M^{-1} K)\phi_i = \lambda_i^2 \phi_i \quad (23)$$

Based on the complex modal theory, the conjugated relations concerned eigenvalues and eigenvectors may be constructed as

$$[M^{-1}K \quad M^{-1}C] \begin{bmatrix} \Phi & \Phi^* \\ \Phi\Lambda & \Phi^*\Lambda^* \end{bmatrix} = -[\Phi\Lambda^2 \quad \Phi(\Lambda^*)^2] \quad (24)$$

$$[K \quad C] = -M[\Phi\Lambda^2 \quad \Phi^*(\Lambda^*)^2] \begin{bmatrix} \Phi & \Phi^* \\ \Phi\Lambda & \Phi^*\Lambda^* \end{bmatrix}^+ \quad (25)$$

where  $\begin{bmatrix} \Phi & \Phi^* \\ \Phi\Lambda & \Phi^*\Lambda^* \end{bmatrix}^+$  is the generalized inverse matrix of  $\begin{bmatrix} \Phi & \Phi^* \\ \Phi\Lambda & \Phi^*\Lambda^* \end{bmatrix}$

The continuous system state matrix may be expressed as

$$A = \begin{bmatrix} 0 & I \\ -K & -C \end{bmatrix} \quad (I \text{ is an identity matrix}) \quad (26)$$

According to the above procedures, the system state-space matrix can be obtained based on the collected displacements or accelerations time histories at different wind velocities. Modal parameters like amplitude, frequency, decaying ratio, and phase angle can be acquired via eigenvalue decomposition.

The above procedures are programmed and the precision as well as the applicability is verified by one numerical example before being utilized to the actual engineering problems.

### 3. Mathematical model for flutter derivative extraction

Since the flutter derivatives signs are related to the directions of self-excited forces and the displacement, whereas the coordinate system definitions may be distinct to different researchers (Scanlan 1993, Sato *et al.* 2002). As a result, the determined flutter derivatives are incomparable, and even result in the wrong application. In this study, the self-excited force and displacement coordinates of bridge deck section is defined in Fig. 1 (Scanlan 1993). The subsequent estimated flutter derivatives and their signs match with Fig. 1.

Under the action of self-excited forces, i.e., lift (downward), drag (downwind) and pitching moment (nose-up), the mathematical model of vertical, torsional and lateral (3-DOF) motion of bridge deck can be expressed in the following form of coupled differential equations.

$$\begin{aligned} m(\ddot{h} + 2\xi_h\omega_h\dot{h} + \omega_h^2h) &= \rho U^2 B \left[ KH_1^* \frac{\dot{h}}{U} + KH_2^* \frac{B\dot{\alpha}}{U} + K^2 H_3^* \alpha + K^2 H_4^* \frac{h}{B} + KH_5^* \frac{\dot{p}}{U} + K^2 H_6^* \frac{p}{B} \right] \\ I(\ddot{\alpha} + 2\xi_\alpha\omega_\alpha\dot{\alpha} + \omega_\alpha^2\alpha) &= \rho U^2 B^2 \left[ KA_1^* \frac{\dot{h}}{U} + KA_2^* \frac{B\dot{\alpha}}{U} + K^2 A_3^* \alpha + K^2 A_4^* \frac{h}{B} + KA_5^* \frac{\dot{p}}{U} + K^2 A_6^* \frac{p}{B} \right] \\ m(\ddot{p} + 2\xi_p\omega_p\dot{p} + \omega_p^2p) &= \rho U^2 B \left[ KP_1^* \frac{\dot{h}}{U} + KP_2^* \frac{B\dot{\alpha}}{U} + K^2 P_3^* \alpha + K^2 P_4^* \frac{h}{B} + KP_5^* \frac{\dot{p}}{U} + K^2 P_6^* \frac{p}{B} \right] \end{aligned} \quad (27)$$

where  $m$  and  $I$  are the model mass and mass inertia moment per unit length, respectively;  $\xi_h$ ,  $\xi_p$ , and  $\xi_\alpha$  are the mechanical damping ratios in vertical, lateral bending and torsion, respectively;  $\omega_h$ ,  $\omega_p$ , and  $\omega_\alpha$  are corresponding natural mechanical frequencies, respectively;  $h$ ,  $p$ ,  $\alpha$ ,  $\dot{h}$ ,  $\dot{p}$ ,  $\dot{\alpha}$ ,  $\ddot{h}$ ,  $\ddot{p}$ ,  $\ddot{\alpha}$  are displacements, velocities and accelerations of vertical, lateral bending, torsional movement, respectively;  $\rho$  is the air density; flutter derivatives  $H_i^*$ ,  $P_i^*$ , and  $A_i^*$  ( $i=1, 2, 3, 4, 5, 6$ ) are functions of the reduced frequency  $K$ ;  $K$  is the product of the motion frequency  $\omega$  and the model

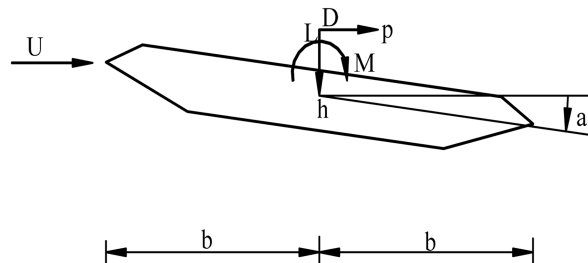


Fig. 1 Self-excited force and displacement coordinates

width  $B$  scaled by the mean oncoming wind velocity  $U$ .

Eq.(27) can be rewritten as

$$\begin{aligned} \ddot{h} + 2\xi_h\omega_h\dot{h} + \omega_h^2h &= H_1\dot{h} + H_2\dot{\alpha} + H_3\alpha + H_4h + H_5\dot{p} + H_6p \\ \ddot{\alpha} + 2\xi_\alpha\omega_\alpha\dot{\alpha} + \omega_\alpha^2\alpha &= A_1\dot{h} + A_2\dot{\alpha} + A_3\alpha + A_4h + A_5\dot{p} + A_6p \\ \ddot{p} + 2\xi_p\omega_p\dot{p} + \omega_p^2p &= P_1\dot{h} + P_2\dot{\alpha} + P_3\alpha + P_4h + P_5\dot{p} + P_6p \end{aligned} \quad (28)$$

where

$$\begin{aligned} H_1 &= \frac{\rho B^2 \omega_h}{m} H_1^*(K), & H_2 &= \frac{\rho B^3 \omega_\alpha}{m} H_2^*(K), & H_3 &= \frac{\rho B^3 \omega_\alpha^2}{m} H_3^*(K) \\ H_4 &= \frac{\rho B^2 \omega_h^2}{m} H_4^*(K), & H_5 &= \frac{\rho B^2 \omega_p}{m} H_5^*(K), & H_6 &= \frac{\rho B^2 \omega_p^2}{m} H_6^*(K) \\ A_1 &= \frac{\rho B^3 \omega_h}{I} A_1^*(K), & A_2 &= \frac{\rho B^4 \omega_\alpha}{I} A_2^*(K), & A_3 &= \frac{\rho B^4 \omega_\alpha^2}{I} A_3^*(K), \\ A_4 &= \frac{\rho B^3 \omega_h^2}{I} A_4^*(K), & A_5 &= \frac{\rho B^3 \omega_p}{I} A_5^*(K), & A_6 &= \frac{\rho B^3 \omega_p^2}{I} A_6^*(K) \\ P_1 &= \frac{\rho B^2 \omega_h}{m} P_1^*(K), & P_2 &= \frac{\rho B^3 \omega_\alpha}{m} P_2^*(K), & P_3 &= \frac{\rho B^3 \omega_\alpha^2}{m} P_3^*(K) \\ P_4 &= \frac{\rho B^2 \omega_h^2}{m} P_4^*(K), & P_5 &= \frac{\rho B^2 \omega_p}{m} P_5^*(K), & P_6 &= \frac{\rho B^2 \omega_p^2}{m} P_6^*(K) \end{aligned}$$

If the displacement vector is given as  $X(t) = [h(t) \ \alpha(t) \ p(t)]^T$ , Eq. (28) may be rewritten concisely in the matrix form

$$\ddot{X} + C^e \dot{X} + K^e X = 0 \quad (29)$$

$$\text{where, } C^e = \begin{bmatrix} 2\xi_h\omega_h - H_1 & -H_2 & -H_5 \\ -A_1 & 2\xi_\alpha\omega_\alpha - A_2 & -A_5 \\ -P_1 & -P_2 & 2\xi_p\omega_p - P_5 \end{bmatrix} \quad K^e = \begin{bmatrix} \omega_h^2 - H_4 & -H_3 & -H_6 \\ -A_4 & \omega_\alpha^2 - A_3 & -A_6 \\ -P_4 & -P_3 & \omega_p^2 - P_6 \end{bmatrix}.$$

$C^e$  and  $K^e$  are the damping and stiffness matrices of the wind-model system.

Eq. (29) can be rewritten as

$$\dot{Y} = AY \quad (30)$$

where,  $Y = [x, \dot{x}]^T$  is the state vector,  $A = \begin{bmatrix} 0 & I \\ -K^e & -C^e \end{bmatrix}$ , which is similar to Eq.(26).

So far, the flutter derivatives at different reduced wind velocities can be obtained easily according to the obtained damping matrix  $C^e$  and stiffness matrix  $K^e$  with those in still air (i.e., inherent

$$\text{mechanical matrices } C^0 = \begin{bmatrix} 2\xi_h\omega_h & & \\ & 2\xi_\alpha\omega_\alpha & \\ & & 2\xi_p\omega_p \end{bmatrix}, K^0 = \begin{bmatrix} \omega_h^2 & & \\ & \omega_\alpha^2 & \\ & & \omega_p^2 \end{bmatrix}.$$

It is necessary to mention that both  $C^0$  and  $K^0$  are both diagonal matrices under the condition with

omitted modal coupling. However, the modal coupling exists among different modes of almost all tests, so the non-diagonal elements in matrices  $C^0$  and  $K^0$  may not equal to zero, especially in 3-DOF section models with attack angle and full bridge aeroelastic models. In the ensuing extracted flutter derivatives, the non-zero portion should be subtracted, or the errors will be inevitably incorporated.

#### 4. Simulation example for modal parameter identification

##### 4.1. Numerical example description

Consider a 3-DOF structure system with independent modes, the vibration equilibrium equation is written as

$$\begin{bmatrix} 1 & & \\ & 1 & \\ & & 1 \end{bmatrix} \{\ddot{X}\} + \begin{bmatrix} 0.4 & & \\ & 0.4 & \\ & & 0.1 \end{bmatrix} \{\dot{X}\} + \begin{bmatrix} 9 & & \\ & 4 & \\ & & 1 \end{bmatrix} \{X\} = 0 \tag{31}$$

For this system, if it is immersed in flows at certain wind velocity, the self-excited forces may occur, and the state-space matrix will change. A bridge deck section model may be assumed to be characterized by the unity mass, inertia and width. Under certain circumstances, the corresponding vibration equilibrium equation may be rewritten as

$$\begin{bmatrix} 1 & & \\ & 1 & \\ & & 1 \end{bmatrix} \{\ddot{X}\} + \begin{bmatrix} 0.5 & 0.2 & 0.2 \\ 0.2 & 0.5 & 0.2 \\ 0.2 & 0.2 & 0.2 \end{bmatrix} \{\dot{X}\} + \begin{bmatrix} 10 & 1 & 1 \\ 1 & 5 & 1 \\ 1 & 1 & 1 \end{bmatrix} \{X\} = 0 \tag{32}$$

For the two states, the modal parameters (frequencies and damping ratios) are calculated and listed in Table 1.

##### 4.2. Parameters identification and analysis

In the following, the accuracy and effectiveness of SST and the corresponding identification programs are demonstrated by utilizing the above system(Eq. (32)). This system is excited by impulse action, and the displacement responses (see Fig. 2, contaminated by noise) are recorded for

Table 1 Modal frequencies and damping ratios for two states

Parameters	$\omega_\alpha$ (rad/s)	$\omega_h$ (rad/s)	$\omega_p$ (rad/s)	$\xi_a$ (%)	$\xi_h$ (%)	$\xi_p$ (%)
Eq.(31)	3	2	1	6.66	10	5
Eq.(32)	3.1960	2.2364	0.8395	9.8562	10.3100	6.4827
0	3.1960	2.2364	0.8395	9.8562	10.3100	6.4827
$\sigma_N/\sigma_S$	0.1	3.1968	2.2463	0.8313	9.9637	10.5076
	0.2	3.1880	2.2470	0.8143	9.9968	10.4526

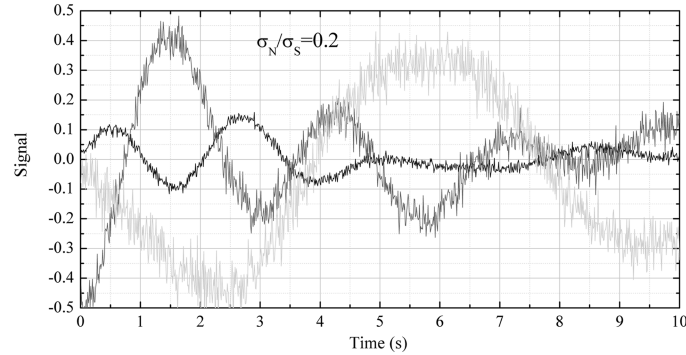


Fig. 2 Ill-conditioned decaying signals contaminated by noise

10s at 0.01s interval. The three sets of records are taken as both reference and non-reference outputs. The structural damping and stiffness matrices are constructed by using SST, and the results are listed in Table 2. The eighteen flutter derivatives are extracted and provided in Table 3. The theoretical flutter derivatives can be directly obtained by subtracting Eq.(31) from Eq.(32) and dividing the corresponding parameters in Eq.(28). They are also offered in Table 3 for the further comparison.

Table 2 Identification results of modal parameters using SST

Parameters	$c_{11}$ $k_{11}$	$c_{12}$ $k_{12}$	$c_{13}$ $k_{13}$	$c_{21}$ $k_{21}$	$c_{22}$ $k_{22}$	$c_{23}$ $k_{23}$	$c_{31}$ $k_{31}$	$c_{32}$ $k_{32}$	$c_{33}$ $k_{33}$
Theoretical values	0.500 10.00	0.200 1.000	0.200 1.000	0.200 1.000	0.500 5.000	0.200 1.000	0.200 1.000	0.200 1.000	0.200 1.000
0	0.500 10.00	0.200 1.000	0.200 1.000	0.200 1.000	0.500 5.000	0.200 1.000	0.200 1.000	0.200 1.000	0.200 1.000
$\frac{\sigma_N}{\sigma_S}$ 0.1	0.494 9.973	0.189 1.012	0.199 1.013	0.225 1.042	0.510 5.044	0.219 1.004	0.199 1.196	0.228 1.122	0.220 1.027
0.2	0.472 9.949	0.180 1.022	0.302 1.045	0.207 0.999	0.489 5.027	0.207 1.013	0.257 1.300	0.334 1.196	0.253 1.027

Table 3 Identification results of flutter derivatives using SST

Parameters		1	2	3	4	5	6
Theoretical values	$H_i^*$	-0.03650	-0.05108	-0.07991	-0.16321	-0.19449	-1.15850
	$A_i^*$	-0.07300	-0.02554	-0.07991	-0.16321	-0.19449	-1.15852
	$P_i^*$	-0.07300	-0.05108	-0.07991	-0.16321	-0.09736	0
Computational values	$H_i^*$	-0.03649	-0.05107	-0.07992	-0.16326	-0.19462	-1.15850
	$A_i^*$	-0.07301	-0.02555	-0.07998	-0.16324	-0.19442	-1.15852
	$P_i^*$	-0.07300	-0.05107	-0.07992	-0.16323	-0.09356	0

For checking the noise-immune performance of the SST program, the original signals are contaminated by introducing Gaussian white noise where the noise-to-signal ratio (refer to  $\sigma_N/\sigma_S$  in this study, where  $\sigma_N, \sigma_S$  are respectively RMS values of noise and original signals, respectively) was specified as 10% and 20% (assuming the similar noise levels are in the response records in wind tunnel test). The identified modal parameter results based on the contaminated signals are listed in Table 1 and Table 2. If the contaminated records are digitally filtered and the high-frequency components are removed (such manipulation is feasible for the real wind tunnel tests), the theoretical targets can also be achieved closely. Similar precision of the flutter derivatives, which have been omitted here for the sake of brevity, can also be obtained. Once the precision of the stiffness and damping matrices is ensured, the flutter derivatives accuracy is undoubtedly satisfactory.

From Table 1, Table 2 and Table 3, it can be observed that the theoretical solutions can be found out by SST if the signal is not contaminated by any noise. Thus the computational accuracy, the validity of SST, and the programs are verified. The parameter errors basically increased with the rising noise level. In addition, poor accuracy of  $c_{13}, c_{31}, c_{32}, k_{31}, k_{32}$  can be detected. The similar characteristics can also be found in Bartoli *et al.*(2009). The major cause may be the weak coupling between vertical mode and lateral mode, torsional mode and lateral mode. Consequently, the corresponding flutter derivatives are sensitive to signal quality and noise, and the phenomena reflect the actual conditions of most bridge decks in wind tunnel tests.

It should be mentioned that the identification results are related to the stochastic response, the random noise, and the lengths of the ‘past’ and ‘future’ data. On the whole, the steady identification results can be acquired by SST; the computational precision and speed are satisfactory. Encouraged by the success of parameters identification by using SST in the numerical simulation example, we can further utilize SST to carry out the identification of modal parameters and flutter derivatives for the actual bridge decks in wind tunnel tests.

### 4.3 Stabilization diagram for frequency and damping

Stabilization diagram is a very important tool. The inherent modes can be firstly distinguished intuitively according to the stabilization diagrams, then calculate the stiffness and damping matrices, and the state matrix can be constructed subsequently. If the results of modal parameters

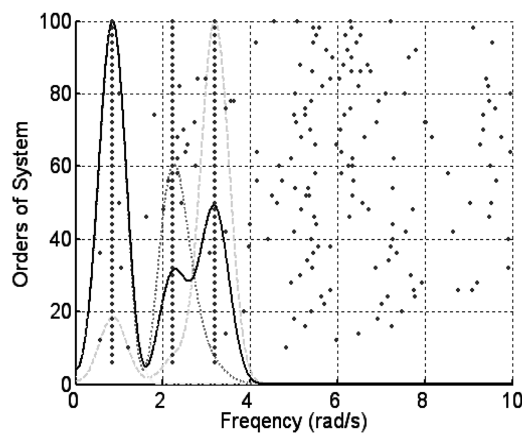


Fig. 3 Frequency stabilization diagram

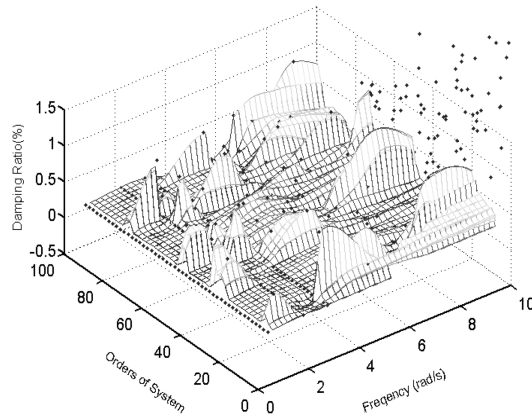


Fig. 4 Damping ratios stabilization diagram

identification are unstable, it may owe to the mingled color noises, the non-linear and non-stationary characteristics of the signals. Figs. 3 and 4 respectively depicts the frequency and damping ratios' stabilization diagrams with noise-free signals.

The curves of three auto power-spectra-density are also plotted. In any the system order, three steady frequencies appear all the time. They are almost equal to those frequencies corresponding to the peak values of the auto power-spectra-density. There are many pseudo modes in the interval of  $0 \sim 10$  rad/s. Also, there are three types of stable damping ratios assembled in three lines, by which the inherent modes frequencies and damping ratios can be distinguished. The damping ratios are marked with bold dots. The grids are fitted and interpolated with the calculated damping ratios. The damping ratios of some scattered dots located at the top right corner are relatively higher and the corresponding frequencies are above  $10$  rad/s. Thus the corresponding modes are factitious.

The simulation example reveals that the identification precision is very satisfactory. Thus the reliability and applicability of the technique as well as the developed programs are verified. At the same time, the above numerical example may be regarded as one benchmark for verifying any identification techniques.

## 5. Parameter identification of bridge deck models in wind tunnel test

### 5.1 Experimental wind tunnel and test setup

The wind tunnel tests are carried out in TJ-1 boundary layer wind tunnel at Tongji University in China. This wind tunnel is an open boundary layer one with a work section of  $1.8$  m (width)  $\times$   $1.8$  m (height), and the wind velocity can be continuously adjusted between  $0.5 \sim 25$  m/s. In this study, the bridge deck section model is suspended with 8 vertical springs and 4 horizontal springs (as depicted in Fig. 5).

The vertical and horizontal motion time histories  $s_1(t)$ ,  $s_2(t)$ ,  $s_3(t)$ ,  $s_4(t)$ ,  $s_5(t)$  at different wind velocities are collected with 5 laser displacement sensors (ANR1282, with the measuring range of  $\pm 20$  mm and the linearity error of 0.2%, among which 3 sensors are for the vertical displacements and the other 2 sensors are for horizontal displacements). The vertical bending displacement can be

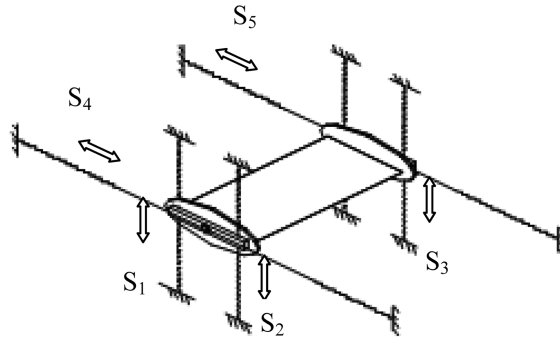


Fig. 5 Schematics of a bridge deck section model

calculated to be the average of  $s_1(t)$  and  $s_3(t)$  (vertical signals), and the torsional displacement can be acquired by the sum of  $s_1(t)$  and  $s_2(t)$  scaled by the distance between the two corresponding sensors. The lateral bending displacement is the average of  $s_4(t)$  and  $s_5(t)$  (horizontal signals). All the signal means are removed from the time histories before applying to parameters identification. In general,  $s_1(t)$ ,  $s_3(t)$  and  $s_4(t)$  are necessary and sufficient in most cases. In our experiments, two additional sensors are setup to simultaneously record the signals for checking the possibility of model torsional motion around the other two axes. The correlation (refers to Eq.(33) between  $s_1(t)$  and  $s_2(t)$ ,  $s_1(t)$  and  $s_3(t)$ ,  $s_2(t)$  and  $s_3(t)$ ,  $s_4(t)$  and  $s_5(t)$  can be determined, and the ideal values should be -1,-1,1,1, respectively, by which the testing signal quality can be examined to offer the precautions for the signal employment. The self-excited force and displacement coordinates are depicted in Fig. 1.

$$r(i, j) = \frac{\sum (s_i - \bar{s}_i)(s_j - \bar{s}_j)}{\sqrt{\sum (s_i - \bar{s}_i)^2 \cdot \sum (s_j - \bar{s}_j)^2}} \quad (33)$$

### 5.2 Features of section models

Two typical cross sections of bridge decks are investigated in this study. One is a streamlined type, i.e., Sutong Bridge (a cable-stayed bridge with main span of 1088 m in China, which is also the largest span for the same bridge style in the world until now) deck (see Fig. 6), and the other is a bluff  $\Pi$  type, i.e., Suramadu Bridge (a cable-stayed bridge with the main span of 434 m in Indonesia, which is the largest span bridge in Southeast Asia at present) deck (see Fig. 7).

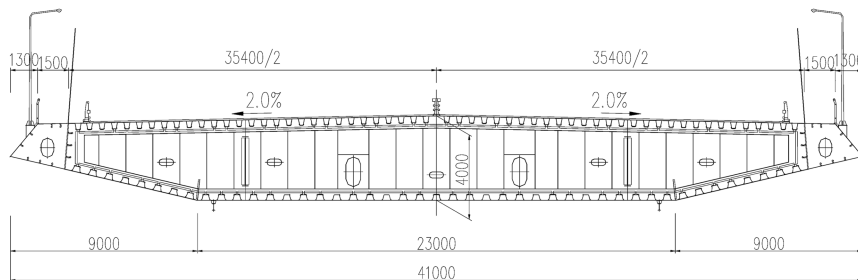


Fig. 6 The cross section of the Sutong Bridge deck (unit: mm)

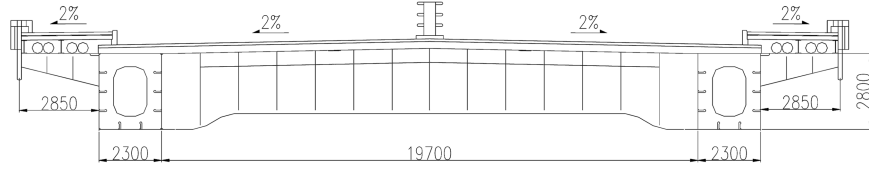


Fig. 7 The cross section of the Suramadu Bridge deck (unit: mm)

Table 4 Relevant parameters for section models of Sutong Bridge and Suramadu Bridge decks

Bridge/Stage	Scale	$L$ (mm)	$B$ (mm)	$H$ (mm)	$m$ (kg/m)	$I$ ( $kg \cdot m^2/m$ )
Sutong/Erection	1 : 50	1700	820	80	15.78	2.950
Suramadu/Service	1 : 50	1700	600	66.5	9.64	0.407
Bridge/State	$\omega_h$ (rad/s)	$\omega_a$ (rad/s)	$\omega_p$ (rad/s)	$\xi_h$	$\xi_a$	$\xi_p$
Sutong/Erection	9.23	15.99	7.37	0.0037	0.0015	0.0037
Suramadu/Service	12.94	22.67	9.12	0.0023	0.0031	0.0032
Bridge/State	$C_D$	$C_L$	$C_M$	$C'_D$	$C'_L$	$C'_M$
Sutong/Erection	0.0295	-0.2615	0.0135	-0.0493	3.982	1.1402
Suramadu/Service	0.13555	-0.11	0.042	-0.2217	5.02	0.7448

Based on the theory of similarity, design parameters for Sutong Bridge (denoted by ‘B1’) and Suramadu Bridge (denoted by ‘B2’) section models can be determined, as listed in Table 4. The initial attack angles are both  $0^\circ$ , and the aerostatic force (i.e., drag, lift and twist moment, see Fig. 1) coefficients ( $C_D, C_L, C_M$ , all with deck width  $B = 2b$  as the reference size, see Fig. 8) and the derivatives ( $C'_D = dC_D/d\alpha, C'_L = dC_L/d\alpha, C'_M = dC_M/d\alpha$ ) about the attack angle may be

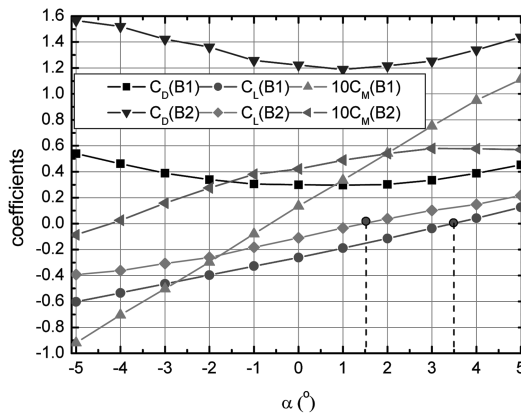


Fig. 8 Aerostatic coefficients

easily achieved.

For the two section models, the testing wind velocities respectively ranges from 3 m/s to 14 m/s and 2 m/s to 10 m/s in smooth flows. The free vibrations are excited by the impulse excitation (initial displacement). Evidently, the amplitude of the decaying signal decreases with time, and consequently the noise-to-signal ratio increases. Therefore, the subsequent records below specific amplitudes (e.g., 2 mm for horizontal and vertical responses and  $0.5^\circ$  for torsional angle) were discarded to improve the estimation accuracy. The absolute values of correlation between  $s_1(t)$  and  $s_2(t)$ ,  $s_1(t)$  and  $s_3(t)$ ,  $s_2(t)$  and  $s_3(t)$ ,  $s_4(t)$  and  $s_5(t)$  are mostly in the interval of (0.99, 1), except for the cases at high wind velocities with intolerable high noise-to-signal ratios that can not be effectively circumvented. Therefore, the flows stability and the signal effectiveness are verified.

## 6. Results and analysis

### 6.1 Modal parameters and frequency stabilization diagram

For Sutong Bridge streamlined deck section and Suramadu Bridge bluff deck section, Figs. 9 and 10 show the vertical, lateral bending and torsional modal frequencies and damping ratios estimated by

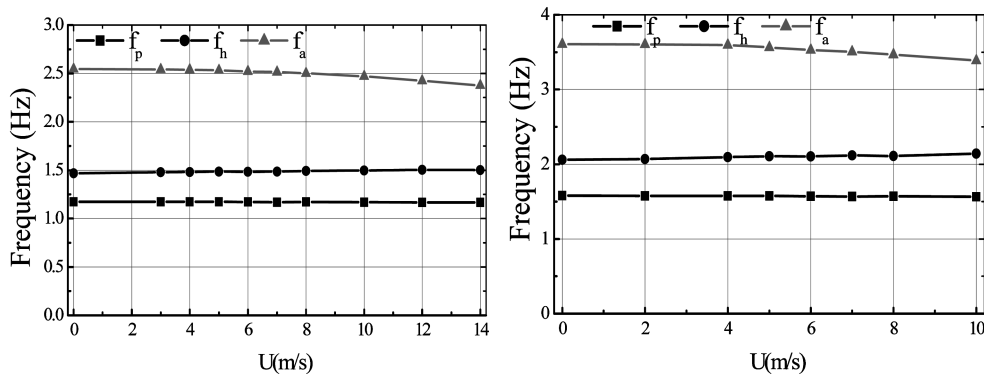


Fig. 9 Modal frequencies (Sutong Bridge and Suramadu Bridge deck models)

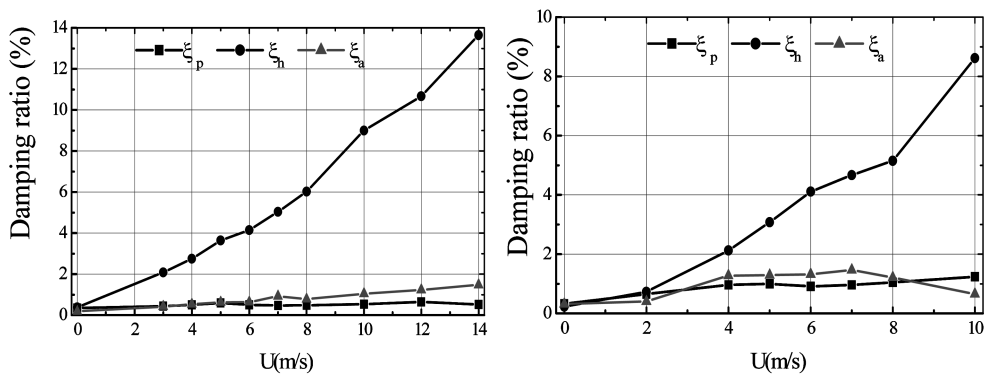


Fig. 10 Modal damping ratios (Sutong Bridge and Suramadu Bridge deck models)

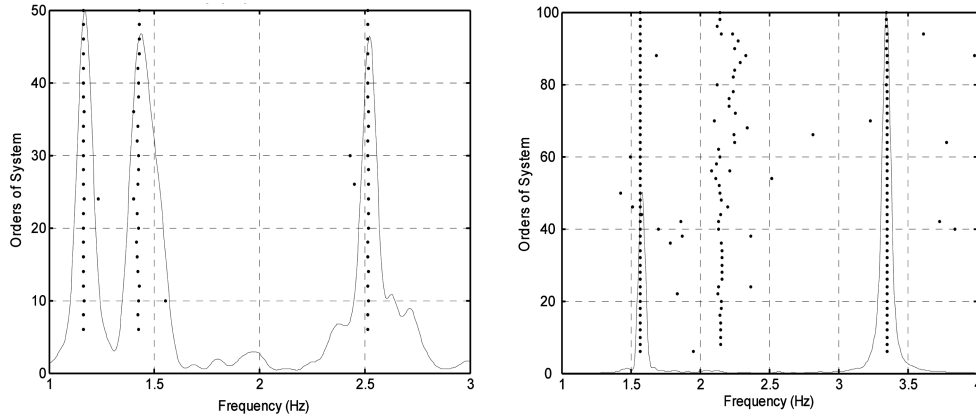


Fig. 11 Frequency stabilization diagram (Sutong Bridge and Suramadu Bridge deck models)

SST. In Eq.(1),  $y^{ref} = \tilde{y}^{ref} = [S_p, S_h, S_\alpha]^T$ , where,  $S_p, S_h, S_\alpha$  are lateral, vertical and torsional responses, respectively.

Some findings: With the increasing wind velocity, the torsional frequencies decrease remarkably, whereas the vertical bending frequencies increase slightly, and the lateral frequencies seem to be consistent. The vertical bending damping ratios increase with the rising wind velocity and approach to 15% and 10%, respectively, at the critical flutter wind velocity. The torsional damping ratios increase to the top of 1.5%, and then decrease to zero at the critical wind velocity. The lateral bending damping ratios increase slowly with wind velocity.

Fig. 11 shows two types of frequency stabilization diagrams of Sutong Bridge and Suramadu Bridge deck vibrating models. If the testing wind velocities are altered, the diagrams will change correspondingly. For Sutong Bridge model, since the wind velocity is low (3 m/s), the modal frequencies at different system orders are very stable. For Suramadu Bridge model, since the wind velocity is higher (10 m/s), which is close to the critical flutter wind velocity, the higher damping ratio of vertical bending induces the poor identification precision, and the modal frequencies at different system orders fluctuate sharply. The diagram shows that the torsional motion component is dominant at this wind velocity. This motion approaches the critical state of torsional flutter. The above phenomena are irrelevant to the identification approach (SST), but more depending on the signal quality.

### 6.2 Flutter derivatives

Fig. 12 provides the 18 flutter derivatives of Sutong Bridge deck section and Suramadu Bridge deck section. Moreover, for a further comparative investigation, flutter derivatives based on the pseudo-steady theory (PST for short) and those of theoretical flat plate (FP for short) are also depicted, which are denoted by ‘PST1’, ‘PST2’ and ‘FP’, respectively. Just as Fig. 9 shows that the modal frequencies change with the testing wind velocity, the corresponding values are utilized to obtain the non-dimensionally reduced velocity in all cases, instead of the zero-wind frequencies.

It must be mentioned that the self-excitation expression adopted in many literatures (Chen *et al.* 2000, Chowdhury *et al.* 2004) is not completely identical for the application of  $\rho U^2 B$  or  $0.5\rho U^2 B$ ,  $k$  or  $K$ ,  $b$  or  $B$ ,  $P_1^* \frac{\dot{h}}{U}$  or  $P_5^* \frac{\dot{h}}{U}$ ,  $P_5^* \frac{\dot{p}}{U}$  or  $P_1^* \frac{\dot{p}}{U}$ ,  $P_4^* \frac{h}{B}$  or  $P_6^* \frac{h}{B}$ ,  $P_6^* \frac{p}{B}$  or  $P_4^* \frac{p}{B}$ , and even the definition of

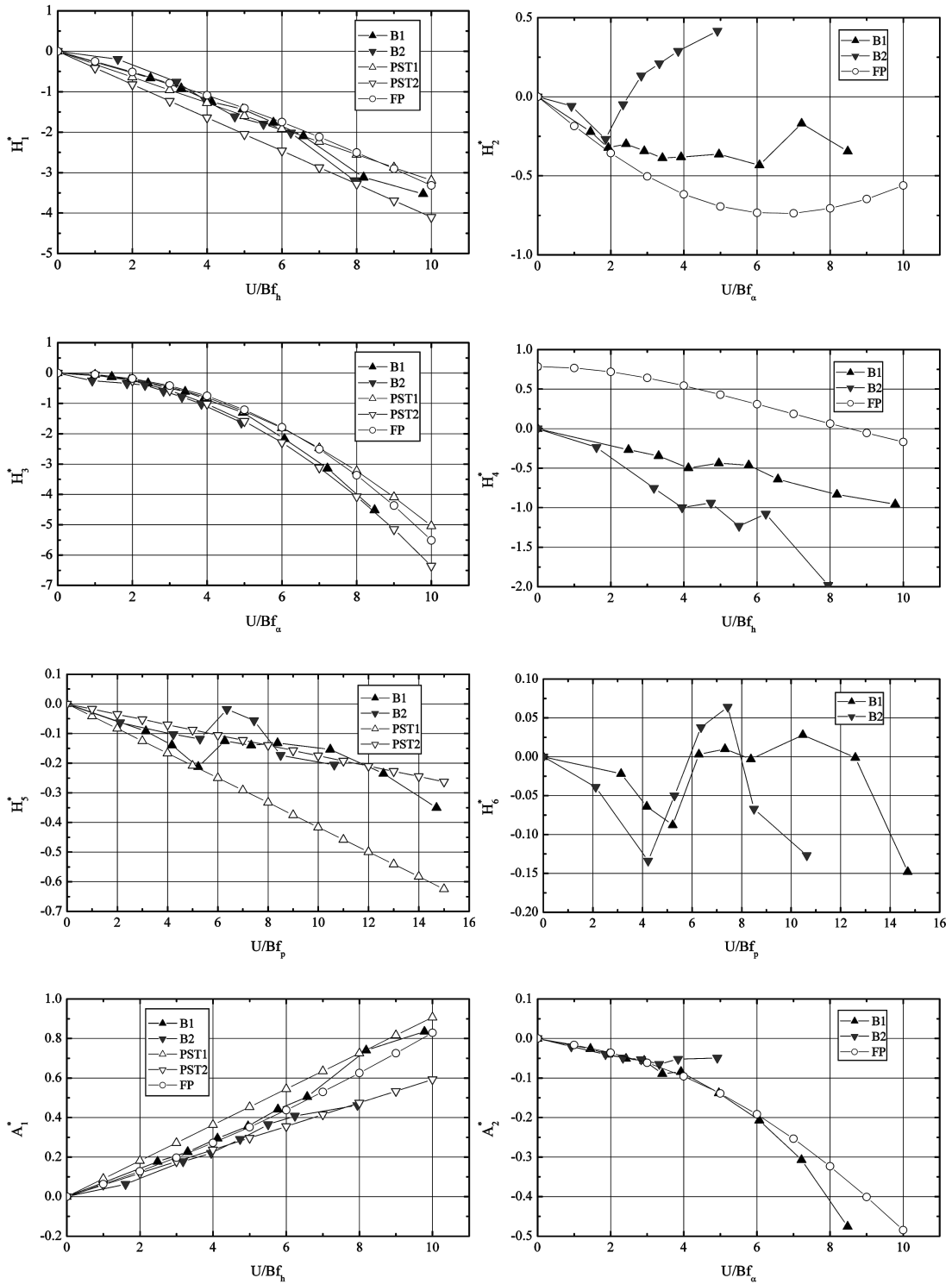


Fig. 12 Flutter derivatives

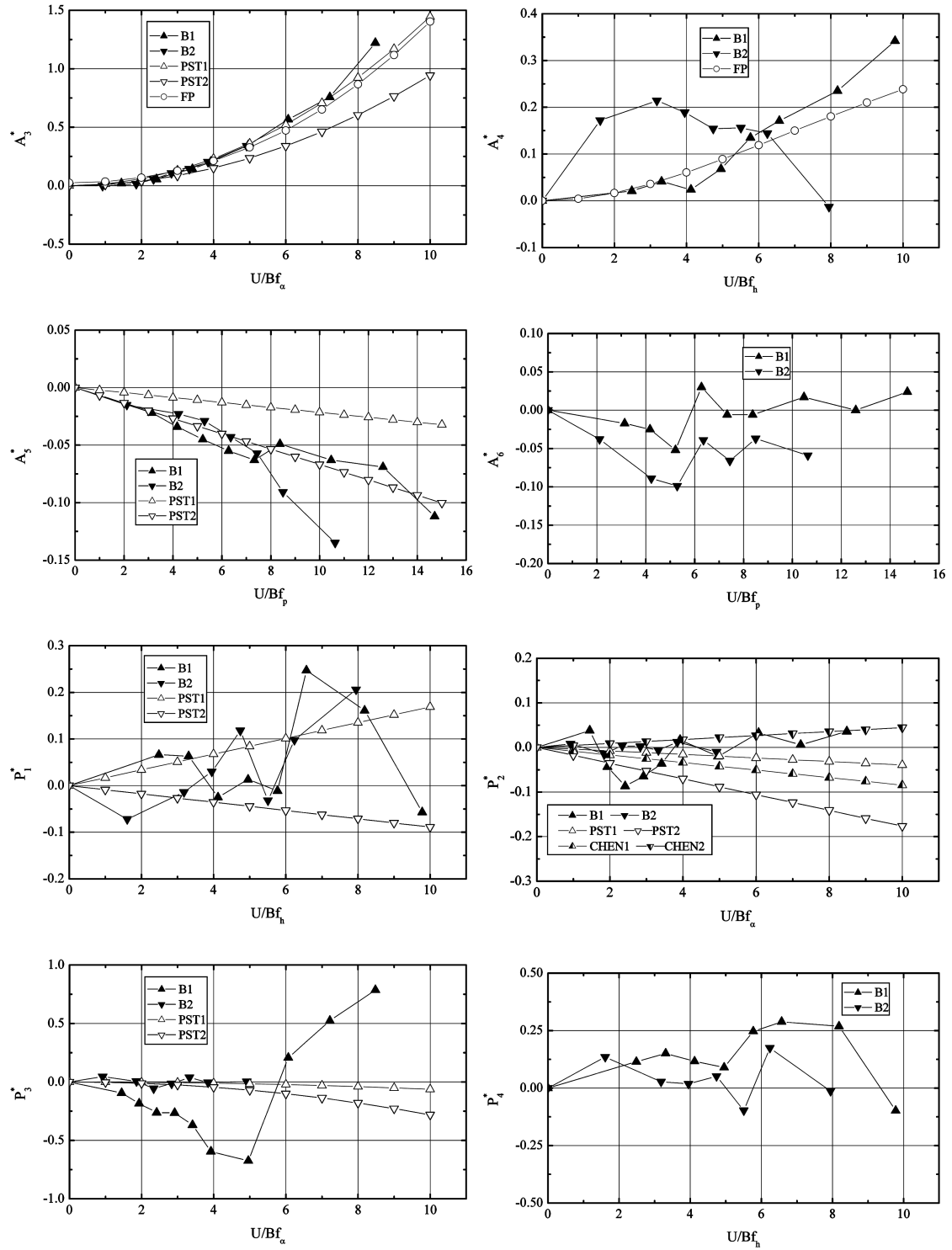


Fig. 12. Continued-1

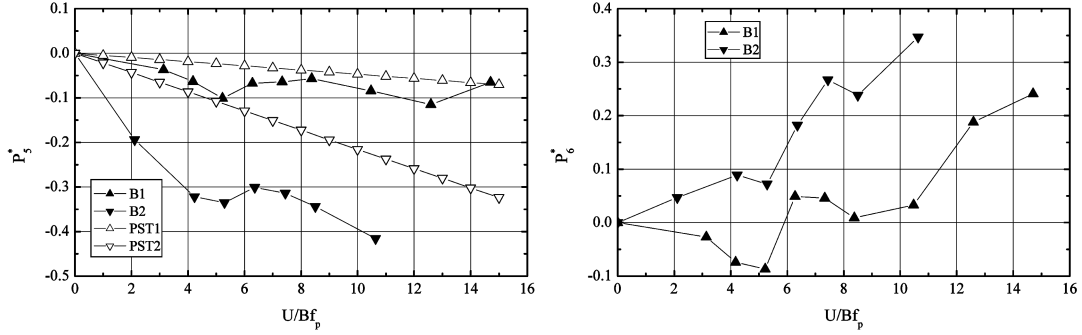


Fig. 12. Continued-2

the coordinates. So the flutter derivatives versus the reduced frequency plots offered in different references may appear “distinct”, which should be consistent with the corresponding formulations.

Pseudo-steady formulation for some flutter derivatives are provided in many literatures (Scanlan 1993, Chen *et al.* 2000, Chowdhury *et al.* 2004) and presented here as (corresponds with Eq.(27))

$$\begin{aligned}
 H_1^* &= -\frac{1}{2K}(C'_L + C'_D); & H_3^* &= -\frac{1}{2K^2}C'_L; & H_5^* &= \frac{1}{K}C_L \\
 A_1^* &= \frac{1}{2K}C'_M; & A_3^* &= \frac{1}{2K^2}C'_M; & A_5^* &= -\frac{1}{K}C_M \\
 P_1^* &= \frac{1}{2K}(C'_D - C'_L); & P_3^* &= \frac{1}{2K^2}C'_D; & P_5^* &= \frac{1}{K}C_D \\
 P_2^* &= \frac{1}{2K}C'_D; & P_4^* &= -\frac{1}{4K}(C'_D - C'_L) = -\frac{P_1^*}{2} \\
 P_4^* &= P_6^* = H_6^* = A_6^* = 0
 \end{aligned} \tag{34}$$

Flutter derivatives  $H_1^*$ ,  $A_1^*$ ,  $H_3^*$ ,  $A_3^*$  are all in good tendency and monotony with the reduced wind velocities for both different section type models. They are all well-matched with the values based on the pseudo-steady formulation and flat plate. If all of them are calculated directly by the flat plate theoretical values only with minor errors, it may be negligible from the actual engineering viewpoint. For the above four types flutter derivatives, the streamlined section (B1) parameters are more close to those of flat plate, which is not difficult to understand. Owing to the relative satisfactory experimental precision of  $C_L$ ,  $C_M$ ,  $C'_L$ ,  $C'_M$  (all of them are not sensitive to section configuration and attack angle compared with  $C_D$  and  $C'_D$ ),  $H_1^*$ ,  $A_1^*$ ,  $H_3^*$ ,  $A_3^*$  based on the pseudo-steady theory are comparatively more stable. An interesting phenomenon is observed: for the two distinct sections, the flutter derivatives' differences between the identification results are lower than those between values derived from pseudo-steady theory. Is it a lucky coincidence or a kind of inevitability? It remains as a pending problem, requiring further investigations and the mysterious mask will finally be unveiled.

For the flutter derivatives related to the lateral self-excitation force, the direct flutter derivatives  $P_5^*$  and  $P_6^*$  are relatively more stable than the other four cross ones, which indicates the similar characteristics for the two types of sections. For  $P_5^*$  and  $P_6^*$ , the experimental and pseudo-steady plots for bridge B2 show a comparatively steeper slope. This particular phenomenon may be result

from the higher drag coefficient generated by the bluff deck. Apparent differences exist in the results ( $P_1^*$ ,  $P_3^*$ ,  $P_5^*$ ,  $H_5^*$ ,  $A_5^*$ ) from the experimental and pseudo-steady theory. In addition, the direct flutter derivative  $P_6^*$  indicates the impact of lateral deflection on the drag aerodynamic force, which should not be set as zero as mentioned in the relevant literature (Chen *et al.* 2000). The above similar phenomena were also observed by Chowdhury *et al.* (2004). These observations may be attributed to both the experimental technique and the pseudo-steady theory.

Cross flutter derivatives  $P_1^*$ ,  $P_2^*$ ,  $P_3^*$  indicate the performances of the vertical velocity, the torsional angular velocity, and the angle effects on the drag aerodynamic force. In consideration of the reality for the experimental sampling with the coupling simultaneous motions in the lateral, vertical, and torsional directions, parameters  $C'_D$  and  $C_L$  are sensitive to the incidence angle (the effective angle incorporating the initial and the additional components). Therefore, the computational accuracy based on the pseudo-steady theory, as well as the experimental identification precision are not satisfactory. Moreover, two distinct formulations for  $P_2^*$  can be referred to Eq. (34). The obvious differences include: the inverse signs, the different denominators, and the different aerostatic coefficients or their derivatives. From the two distinctly even 'strange' expressions, one can conclude that the determination of  $P_2^*$  may be quite difficult. The results obtained from the two formulations are also presented in Fig. 12, in which CHEN1 and CHEN2 represent the results based on  $P_2^* = -1/4K(C'_D - C_L)$  utilized by Chen *et al.*(2000). Just as the predictions, the three set of results are incomparable.

Cross flutter derivatives,  $P_4^*$ ,  $H_6^*$ ,  $A_6^*$  are assumed to be zero by Chen *et al.*(2000). Such an assumption indicates that the vertical deflection has no effect on drag force, and lateral deflection has no effect on lift force and torsional moment either. It is fundamentally reasonable and liable to be accepted. From the plots in Fig. 12, all the experimental results are close to zero without obvious monotonic trend at the reduced velocity, and comply with the assumption.

Flutter derivatives  $H_2^*$  shows the inverse tendency at the reduced wind velocity for two section types. The excitation vertical forces induced by the torsional motion are opposite for Sutong Bridge and Suramadu Bridge deck at higher wind speeds. One plausible reason is the attack angles corresponding to the zero (i.e., separatrix) lift coefficient (see Fig. 8) are about  $3.5^\circ$  and  $1.5^\circ$ , respectively. At higher wind speeds, the added attack angle may exceed  $2^\circ$  for the positive torsional moment (see Fig. 8). During the oscillation course, even at the same attack angle (inclusive of the added angle) state, the orientation of the aerodynamic force caused by the rotation velocity may be different for two sections.

Compared with the deck width, the size of height is much smaller. Therefore, the identification precisions of the flutter derivatives concerning with the lateral motion are unsatisfactory. It should be mentioned that the sharp fluctuations may occasionally appear at the curves of the flutter derivatives versus the reduced wind velocity. Unexpected interruptions may be caused by the contaminated non-ideal signal. It is admittedly that 1-DOF and 2-DOF techniques are more effective in accuracy than that of 3-DOF method. Of course, the subsequent experimental and computational task is more time-consuming.

## 7. Conclusions

The modal parameters and eighteen flutter derivatives of 3-DOF models for two types of typical deck section are simultaneously identified by using the reference-based Stochastic Subspace

Technique. The main conclusions and findings in this study are summarized as follows:

(1) SST is one practical approach for identifying the bridge system modal parameters and the aerodynamic derivatives. If the signals are ideal, i.e., without any external interference and noises, the achieved results may be indefinitely approach the theoretical values, which are verified by a numerical example.

(2) Although the parameter identification may be carried out by using the oscillation signals induced by oncoming or signature turbulence in turbulent and smooth flows, the accuracy can not be effectively ensured. Comparing the identified results in this study with those in the previous investigations, it can be observed that the artificial impulse experimental schemes made by the authors are more feasible and accurate results can be achieved. The experimental procedure seems to be more critical than the identification technique for the estimation precision refining.

(3) Whether for the streamlined deck section or the bluff deck section, the identified values of  $H_1^*$ ,  $H_3^*$ ,  $A_1^*$ ,  $A_3^*$  are all in good consistency with those based on pseudo-steady theoretical values. Therefore, the pseudo-steady theory can provide acceptable estimation for the aforementioned four components. The lateral direct flutter derivatives  $P_5^*$ ,  $P_6^*$  are comparatively more accurate than others related lateral components. The main causes for the poor precision of some flutter derivatives should be ascribe to the negligible coupling, the high noise-to-signal ratio, and the sensitivity to the signal variation. To a great extent, the reasonable and practical experimental setup and procedure play the key roles in the refining of the identification precision of flutter derivatives.

## Acknowledgements

The research is supported by the National Science Foundation of China under Grant No. 50708012 and co-supported by the New Faculty Research Fund for the Doctoral Program of Higher Education by the Ministry of Education of China under Grant No. 20070141073. Both of them are gratefully acknowledged.

## References

- Bartoli, G., Contri, S., Mannini, C. and Righi, M. (2009), "Toward an improvement in the identification of bridge deck flutter derivatives", *J. Eng. Mech - ASCE*, **135**(8), 771-785.
- Chen, A.R., He, X.F. and Xiang, H.F. (2002), "Identification of 18 flutter derivatives of bridge decks", *J. Wind Eng. Ind. Aerod.*, **90**(12-15), 2007-2022.
- Chen, A.R., Xu, F.Y. and Ma, R.J. (2006), "Identification of flutter derivatives of bridge decks using stochastic search technique", *Wind Struct.*, **9**(6), 441-455.
- Chen, X.Z. and Kareem, A. (2004), "Efficacy of the implied approximation in the identification of flutter derivatives", *J. Struct. Eng - ASCE*, **130**(12), 2070-2074.
- Chen, X.Z. and Kareem, A. (2008), "Identification of critical structural modes and flutter derivatives for predicting coupled bridge flutter", *J. Wind Eng. Ind. Aerod.*, **96**(10-11), 1856-1870.
- Chen, X.Z., Matsumoto, M. and Kareem, A. (2000), "Aerodynamic coupling effects on flutter and buffeting of bridges", *J. Eng. Mech - ASCE*, **126**(1), 17-26.
- Chen, Z.Q., Han, Y., Luo, Y.Z. and Hua, X. (2010), "Identification of aerodynamic parameters for eccentric bridge section model", *J. Wind Eng. Ind. Aerod.*, **98**(4-5), 202-214.
- Chowdhury, A.G. and Sarkar, P.P. (2003), "A new technique for identification of eighteen flutter derivatives using a three-degree-of-freedom sectional model", *Eng. Struct.*, **25**(14), 1763-1772.

- Chowdhury, A.G. and Sarkar, P.P. (2004a), "Identification of eighteen flutter derivatives of an airfoil and a bridge deck", *Wind Struct.*, **7**(3), 187-202.
- Gu, M. and Qin, X.R. (2004), "Direct identification of flutter derivatives and aerodynamic admittance of bridge decks from structural random response", *Eng. Struct.*, **26**(14), 2161-2172.
- Gu, M. and Xu S.Z. (2008), "Effect of rain on Flutter derivatives of bridge decks", *Wind Struct.*, **11**(3), 209-220.
- Gu, M., Zhang, R.X. and Xiang, H.F. (2000), "Identification of flutter derivatives of bridge decks", *J. Wind Eng. Ind. Aerod.*, **84**(2), 151-162.
- Li, Y.L., Liao, H.L. and Qiang, S.Z. (2003), "Weighting ensemble least-square method for flutter derivatives of bridge decks", *J. Wind Eng. Ind. Aerod.*, **91**(6), 713-721.
- Ma, R.J. and Chen, A.R. (2007), "Determination of flutter derivatives by a taut strip model", *J. Wind Eng. Ind. Aerod.*, **95**(9-11), 1400-1414.
- Mishra, S.S., Krishen, K. and Prem, S. (2006), "Identification of 18 flutter derivatives by covariance driven stochastic subspace method", *Wind Struct.*, **9**(2), 159-178.
- Peeters, B. and Roeck, G.D. (1999), "Reference-based stochastic subspace identification for output-only modal analysis", *Mech. Syst. Signal Pr.*, **13**(6), 855-878.
- Qin, X.R. and Gu, M. (2004), "Determination of flutter derivatives by covariance-driven stochastic subspace identification technique", *Wind Struct.*, **7**(3), 173-186.
- Qin, X.R., Kwok, K.C.S., Fok, C.H., Hitchcock, P.A. and Xu, Y.L. (2007), "Wind-induced self-excited vibrations of a twin-deck bridge and the effects of gap-width", *Wind Struct.*, **10**(5), 463-479.
- Quan, Y., Gu, M. and Tamura, Y. (2005), "Experimental evaluation of aerodynamic damping of square super high-rise buildings", *Wind Struct.*, **8**(5), 309-324.
- Sarkar, P.P., Gan Chowdhury, A. and Gardner, T.B. (2004b), "A novel elastic suspension system for wind tunnel section model studies", *J. Wind Eng. Ind. Aerod.*, **92**(1), 23-40.
- Sato, H., Hirahara, N., Fumoto, K., Hirano, S. and Kusuhara, S. (2002), "Full aeroelastic model test of a super long-span bridge with slotted box girder", *J. Wind Eng. Ind. Aerod.*, **90**(12-15), 2023-2032.
- Scanlan, R.H. (1993), "Problematic in formulation of wind-force models for bridge decks", *J. Struct. Eng - ASCE*, **119**(7), 1433-1446.
- Singh, L., Jones, N.P., Scanlan, R.H. and Lorendeaux, O. (1996), "Identification of lateral flutter derivatives of bridge decks", *J. Wind Eng. Ind. Aerod.*, **60**(1-3), 81-89.